

LS Scienza dei Materiali - a.a. 2005/06

Fisica delle Nanotecnologie – part 3

Version 4, Oct 2005

Francesco Fuso, tel 0502214305, 0502214293 - fuso@df.unipi.it

<http://www.df.unipi.it/~fuso/dida>

Trasporto per tunneling in quantum dots: Coulomb blockade e single electron devices

3/11/2005 – 16.30-18 – room T1

10/11/2005 – 16.30-18 – room T1

Outlook

- 0DEG (quantum dots) structures will be considered and *single electron* processes will be analyzed (transport inherently related to inter-dot tunneling)
- The simplest way to approach the single electron world: a nanosized capacitor
- *Continuous vs quantized* quantities: the “struggle” between adding a single electron to a nanosized capacitor and adjusting its potential
- Coulomb blockade effects, Coulomb staircase and oscillations
- Three-terminal (active) devices: single electron transistor in conventional and alternative fashions
- Preliminary: discrete energy levels in semiconductor quantum dots (potential wells) and tunneling
- Tunneling through a quantum dot (double barrier): resonant tunneling diodes

Nanosized conductors (an ideal case)

Capacitance of a nanosized conductor (e.g., a metal) sphere



$$\begin{aligned}Q &= C V \\V &= Q/4\pi\epsilon_0 r \\C &= 4\pi\epsilon_0 r \\E &= CV^2/2\end{aligned}$$

Es.: if $r \sim 10$ nm, $C \sim 1$ aF
At $V = 1$ V $Q \sim 10^{-18}$ Coulomb
That is $N \sim 6$ e !!!

The discrete nature of electric charge dominates the behavior of nanosized capacitors

In systems of very small conductors, the capacitances approach values sufficiently small that the charging energy given by (4.47) due to a single electron, $e^2/2C$, becomes comparable to the thermal energy, $k_B T_l$. The transfer of a single electron between conductors therefore results in a voltage change that is significant compared to the thermal voltage fluctuations and creates an energy barrier to the further transfer of electrons. This barrier remains until the charging energy is overcome by sufficient bias. How small must such a structure be? A simple example is the case of a conducting sphere above a grounded conducting plane. This example approximates a metal cluster imbedded in an insulator above a conducting substrate, which is a commonly realized structure that has been extensively studied experimentally. The exact solution may be found using the method of images, which gives the capacitance

Accurate capacitance evaluation for realistic cases

After Ferry and Goodnick,
Transport in nanostructures,
Cambridge (1997)

of the sphere as [33]

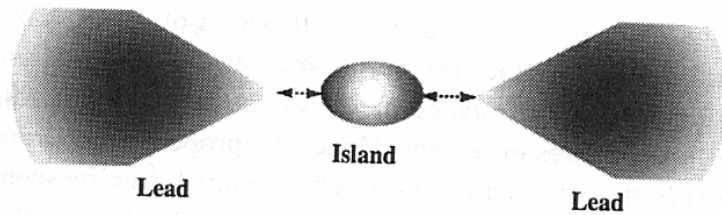
$$C = 4\pi\epsilon a \left(1 + \alpha + \frac{\alpha^2}{1 - \alpha^2} + \dots \right), \quad \alpha = \frac{a}{2l}, \quad (4.50)$$

where a is the radius of the sphere and l is the distance above the conducting substrate. As the radius of the sphere becomes small compared to l , the capacitance becomes independent of the distance of the cluster from the substrate. An alternate example is that of a flat circular disk located parallel to and a distance d above a ground plane. This example is more closely analogous to the semiconductor quantum dots fabricated by lateral confinement of a 2DEG as discussed in the previous sections. The solution is given in a problem in Jackson's textbook [34] (which we leave as an exercise for the reader!), with the capacitance given in the limit of $d \gg R$ as

$$C = 8\epsilon R \quad (4.51)$$

where R is the radius of the disk. Equating the charging energy with the thermal energy, we see that at room temperature, $C \sim 3 \times 10^{-18}$ F. The corresponding radius for a sphere from (4.50) is on the order of $a \sim 28$ nm (assuming a relative dielectric constant of 1), and somewhat larger for the disk. The facts that $\epsilon > \epsilon_0$ in real structures and that the charging energy should be several times larger than the thermal energy imply that sub-10-nm structures need to be fabricated in order to see clear single-electron charging effects at room temperature. Although it is still somewhat challenging with today's lithographic techniques to nanoengineer such structures, it is not difficult to grow insulating films with random metallic clusters on this order in which Coulomb blockade effects are readily observed, even at room temperature. Further, if we perform measurements at cryogenic temperatures, then the size scale becomes comparably larger, allowing single-electron effects to be observed in nanofabricated quantum dot structures.

Tunneling rules the behavior of the system



Tunneling inherently involved when “charging” the capacitor

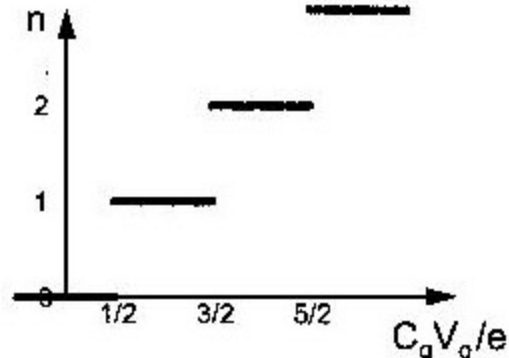


Figure 2: Electron number versus gate voltage characteristics of single-electron box. The number of electron in the quantum dot increases one by one as the gate voltage increases.

$$Q = CV \quad (4.46)$$

where C is the capacitance, Q is the charge on the conductor, and V the electrostatic potential relative to some chosen reference (e.g., ground). Since we are considering an ideal conductor, any charge added to the conductor rearranges itself such that the electric field inside vanishes, and the surface of the conductor becomes an equipotential surface. Therefore, the electrostatic potential associated with the conductor relative to its reference is uniquely defined. If we consider two conductors connected by a d.c. voltage source, a voltage $+Q$ builds up on one conductor and a charge $-Q$ on the other. The capacitance of the two conductor system is then defined as $C = Q/V_{12}$. The electrostatic energy stored in the two conductor system is the work done in building up the charge Q on the two conductors and is given by

$$E = \frac{Q^2}{2C} \quad \text{Electrostatic energy} \quad (4.47)$$

For a system of N conductors, the charge on conductor i may be written

$$Q_i = \sum_{j=1}^N C_{ij} V_j, \quad (4.48)$$

where the diagonal values C_{ii} are the capacitance of conductor i if all other conductors are grounded. The diagonal elements are commonly referred to as the *coefficients of capacitance*; the off-diagonal elements are called the *coefficients of induction*. The total electrostatic energy stored in a multiconductor system is given by the generalization of Eq. (4.47) as

$$E = \frac{1}{2} \sum_i \sum_j (C^{-1})_{ij} Q_i Q_j, \quad (4.49)$$

It is important to note that the polarization charge on the capacitor, Q , does not have to be associated with a discrete number of electrons, N . This charge is essentially due to a rearrangement of the electron gas with respect to the positive background of ions, and as such it may take on a continuous range of values. It is only when we consider changes in this charge due to the tunneling of a single electron between the conductors that the discrete nature becomes apparent.

Discrete (charge) vs continuous (voltage)

Conditions to observe “quantized effects”

Basic Operation of Single-Electron Box

As the size of the quantum dot decreases, the charging energy W_c of a single excess charge on the dot increases. If the quantum-dot size is sufficiently small and the charging energy W_c is much greater than thermal energy $k_B T$, no electron tunnels to and from the quantum dot. Thus, the electron number in the dot takes a fixed value, say zero when both the electrodes are grounded. The charging effect, which blocks the injection/ejection of a single charge into/from a quantum dot, is called Coulomb blockade effect. Therefore, the condition for observing Coulomb blockade effects is expressed as

$$W_c = \frac{e^2}{2C} \gg k_B T, \quad (1)$$

where C is the capacitance of the quantum dot and T is the temperature of the system.

However, it should be noted that by applying a positive bias to the gate electrode we could attract an electron to the quantum dot. The increase of the gate voltage attracts an electron more strongly to the quantum dot. When the gate bias exceeds a certain value an electron finally enters the quantum dot and the electron number of the dot becomes one. Further increase of the gate voltage makes it possible to make the electron number two. Thus, in the single-electron box, the electron number of the quantum dot is controlled one by one, by utilizing the gate electrode (Figure 2).

Conditions for Observing Single-Electron Tunneling Phenomena

In order to observe single-electron tunneling phenomena, or Coulomb blockade effect there are two necessary conditions. One condition is, as described above, that the charging energy of a single excess electron on a quantum dot is much greater than the thermal energy (Eq. (1)). The other condition is that the tunneling resistance R_t of the tunneling junction must be larger than resistance quantum h/e^2 . This condition is required to suppress the quantum fluctuations in the electron number, n , of the dot so that they are sufficiently small for the charge to be well localized on the quantum dot. The condition is obtained by keeping uncertainty principle $\Delta W \Delta t > h$ while letting ΔW be the charging energy of the quantum dot, $\sim e^2/C$, and Δt be the lifetime of the charging, $R_t C$. Then, the uncertainty principle reduces to

$$\Delta W \cdot \Delta t \sim \frac{e^2}{C} \cdot R_t C = e^2 R_t > h. \quad (2)$$

As a result, one obtains the condition for the tunneling resistance R_t in order to observe the Coulomb blockade effects

$$R_t \gg \frac{h}{e^2} = 25.8 \text{ k}\Omega. \quad (3)$$

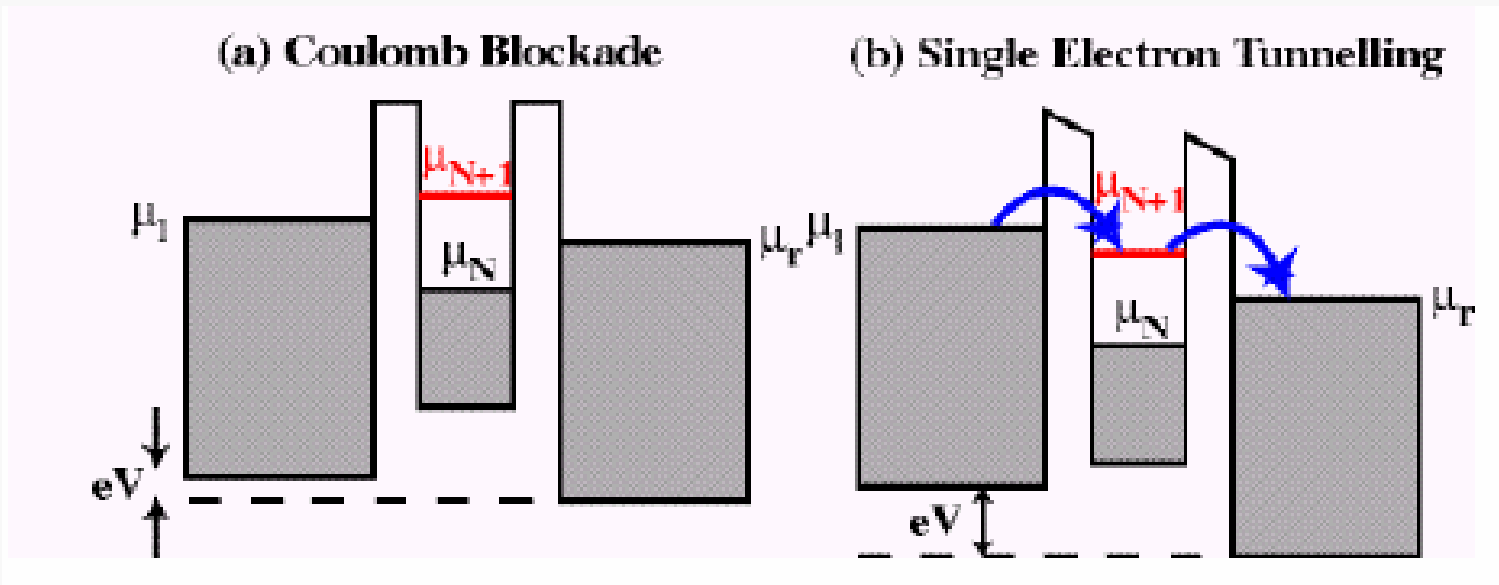
Temperature-related energy fluctuations must be negligible (low T operation!!)

Specific conditions must be fulfilled to realize experimentally the quantum-driven phenomenon

Tunneling resistance must be large enough (*weak coupling*)

Da R. Waser Ed., Nanoelectronics and information technology (Wiley-VCH, 2003)

Coulomb blockade (Cb) and SE tunneling



In quantum mech. terms:

double barrier resonant tunneling

Figure 2.2:- For an island of total capacitance C with N electrons, being μ_N the chemical potential of the highest filled electron state, μ_{N+1} the chemical potential of the first available empty state for an electron and μ_l and μ_r the chemical potentials of the left and right electrodes respectively, it may be shown that the energy to add an electron to the island is $\mu_{N+1} - \mu_N = e^2/C$. Therefore provided $e^2/C \gg k_B T$ (the thermal energy - i.e. C is small) and the tunnelling resistance, $R_T \gg R_Q \approx 25.8 k\Omega$ (i.e. the electron wavefunction may be localised on the island) for a voltage V applied across the electrodes, no electrons may flow if $\mu_{N+1} > \mu_l$ and μ_r , - the state known as Coulomb blockade (a). If a larger bias is applied across the electrodes such that $\mu_l > \mu_{N+1} > \mu_r$, then empty states may be populated in the island and single electrons may tunnel through the island (b). A gate may be used to change the Fermi level of the island and therefore switch the single electron current on or off.

Coulomb blockade: an additional electron is accepted by the dot only if the voltage is raised above some limit

Coulomb oscillations and staircase

Da G. Timp, Nanotechnology (Springer-Verlag, 1999)

After Ferry and Goodnick, Transport in nanostructures, Cambridge (1997)

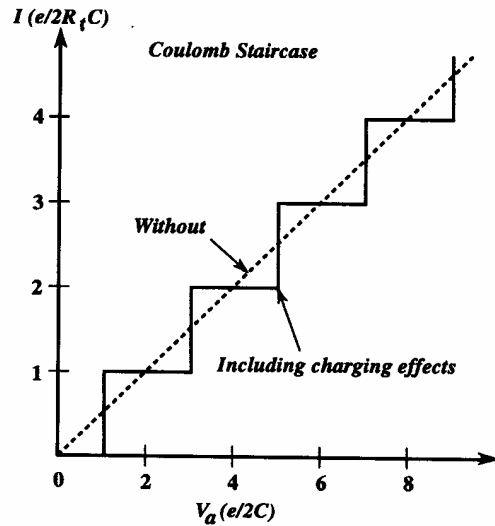


Fig. 4.15. Ideal current-voltage characteristics for an asymmetric double junction system with and without consideration of Coulomb charging effects. For this system, $C_1 = C_2 = C$ and $R_l = R_r \gg$

2

(Discrete) charge effects inhibit continuous charging of the capacitor, i.e., tunneling transport of electrons through the dot

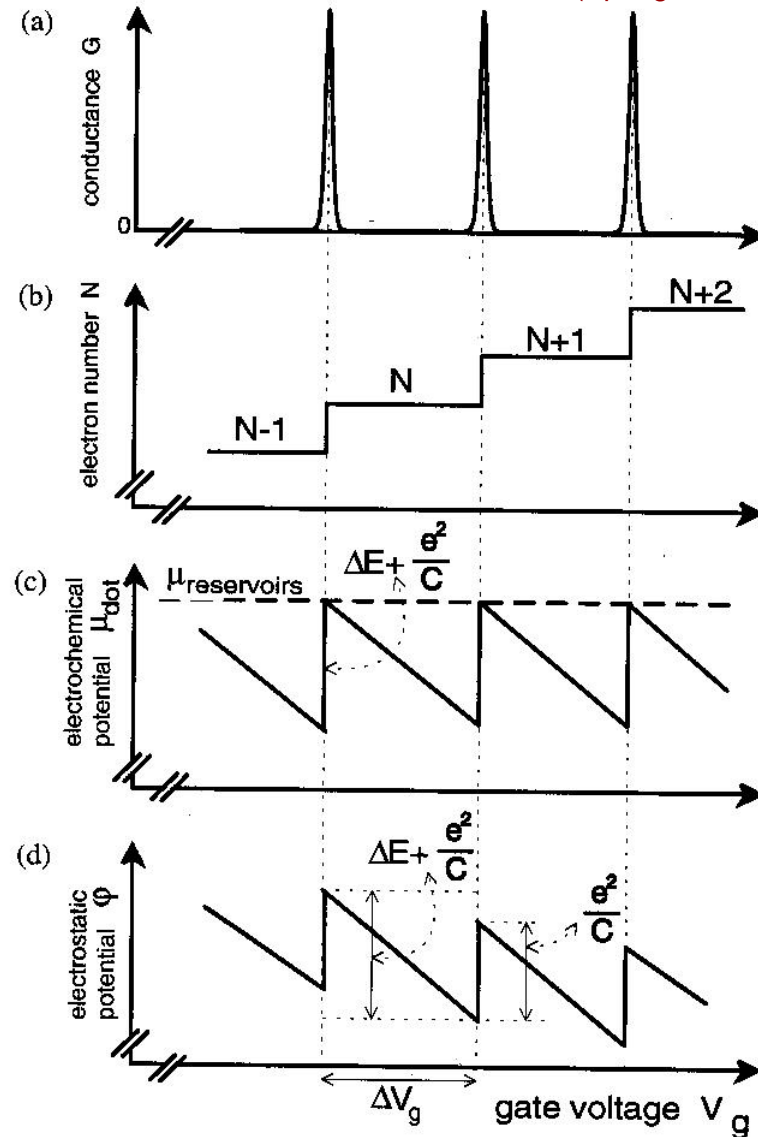
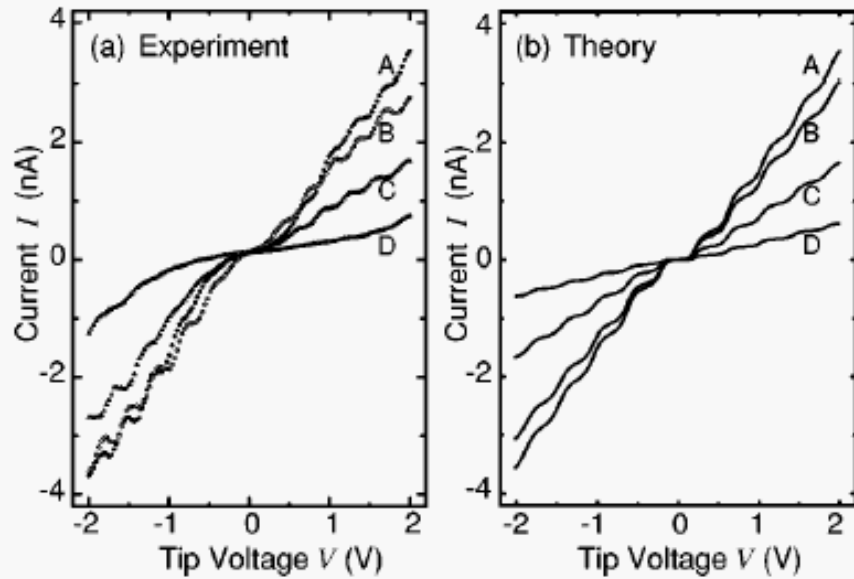


FIGURE 6. Schematic comparison, as a function of gate voltage, between (a) the Coulomb oscillations in the conductance G , (b) the number of electrons in the dot ($N+i$), (c) the electrochemical potential in the dot, $\mu_{dot}(N+i)$, and (d) the electrostatic potential ϕ .

Examples of measurements



See Imamura et al. PRB 61 46 (2000)

FIG. 3. (a) Experimental I - V curves for a 10-nm-thick $\text{Co}_{36}\text{Al}_{22}\text{O}_{42}$ at room temperature. A, B, C, and D refer to different distances between the STM tip from the surface of the sample. The lateral position for A and B is different from that for C and D. (b) Corresponding theoretical curves in a triple tunnel junction system at $T=300$ K. The tunnel resistance at the bottleneck is taken to be $R_1=600, 700, 1300,$ and 3500 M Ω for lines A, B, C, and D, respectively. The other tunnel resistances are $R_2=R_3=1$ M Ω and the capacitances are $C_1=4.48 \times 10^{-19}$ F, $C_2=2.13 \times 10^{-19}$ F, and $C_3=3.62 \times 10^{-19}$ F for all curves.

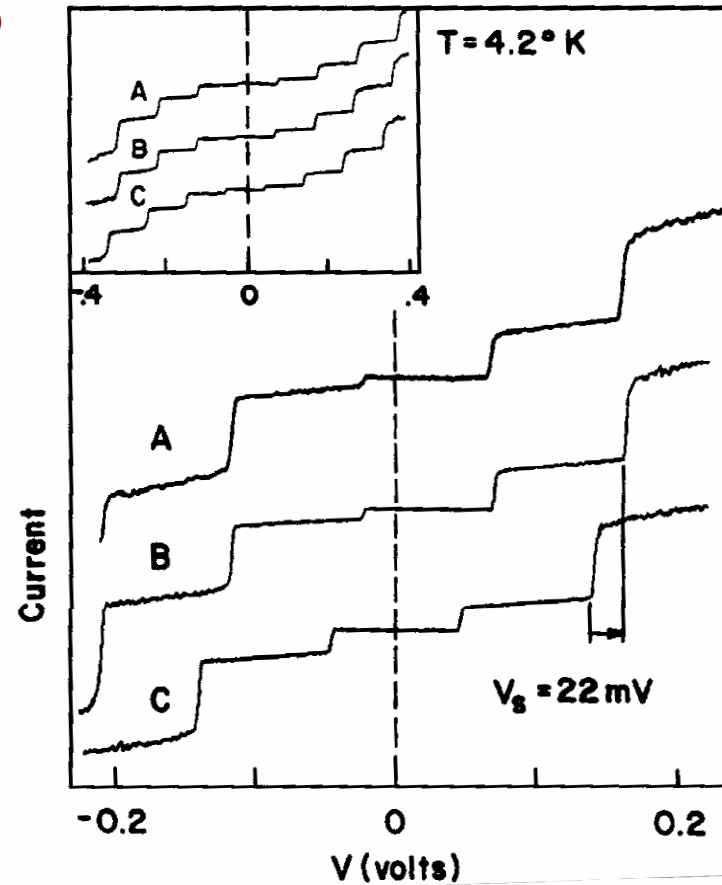
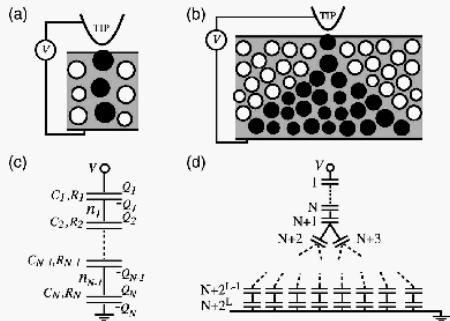


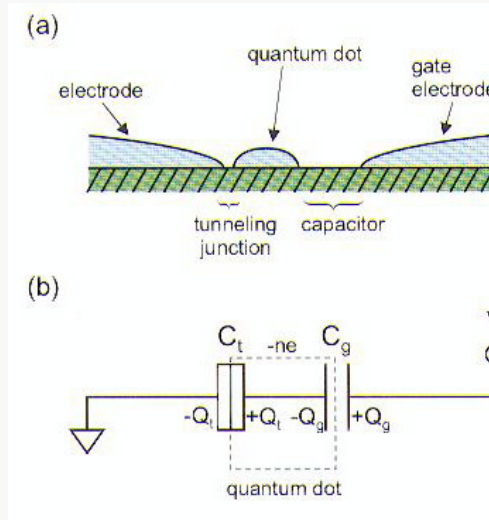
Fig. 4.12. Experimental (A) and theoretical (B and C) I - V characteristics from an STM-contacted 10 nm diameter In droplet illustrating the Coulomb staircase in a double junction system. The peak-to-peak current is 1.8 nA. The curves are offset from one another along the current axis, with the intercept corresponding to zero current. [After Wilkins *et al.*, Phys. Rev. Lett. **63**, 801 (1989), by permission.]



STM measurements
room-temperature
granular metal films
(ϕ 1-10 nm)

STM used to make a point-like tunneling with nanosized dots

Single Electron Transistor (SET)



Bias Conditions for Coulomb Blockade Effects

The voltage range, which keeps the electron number at n in the dot, is extracted by considering the free energy of the system. The free energy of the system having n electron in the island $F(n)$ is expressed as

$$F(n) = W_c(n) - A(n), \quad (6)$$

where $W_c(n)$ is the charging energy and $A(n)$ is the work done by the voltage source connected to the gate electrode in order to make the electron number be from zero to n .

It is important to note that when tunneling phenomena do not occur the tunnel junction behaves as a normal capacitor and that the polarization charge on the capacitor does not have to be associated with a discrete number of electrons, n . This polarization

charge is essentially due to a rearrangement of the electron gas with respect to the positive background of ions. Therefore, the polarization charge takes a continuous range of value, although the number of electrons in the quantum dot takes a discrete number of electrons, n . The polarization charges on the tunneling junction and gate capacitor are obtained from the following relationship.

$$Q_t - Q_g = -ne, \quad (5)$$

$$\frac{Q_t}{C_t} + \frac{Q_g}{C_g} = V_g,$$

where Q_t and Q_g are the polarization charge on the tunneling junction and the gate capacitor, respectively. By using Q_t and Q_g , the charging energy $W_c(n)$ of the quantum dot is expressed as,

$$W_c(n) = \frac{Q_t^2}{2C_t} + \frac{Q_g^2}{2C_g}, \quad (6)$$

which reduces to

$$W_c(n) = \frac{e^2 n^2}{2C_\Sigma} + \frac{1}{2} \frac{C_t C_g V_g^2}{C_\Sigma}, \quad (7)$$

where $C_\Sigma = C_t + C_g$. In addition, the work, $A(n)$, done by the gate voltage source in order to make electron number of the quantum dot be from zero to n is expressed as,

$$A(n) = \int I(t) \cdot V_g dt = Q_g V_g = en \frac{C_g}{C_\Sigma} V_g + \frac{C_t C_g V_g^2}{C_\Sigma}. \quad (8)$$

In order to maintain the electron number in the quantum dot, the following conditions are required.

$$F(n) < F(n \pm 1) \quad (9)$$

From Eqs.(7) to (9), the voltage range, within which Coulomb blockade effects are in effect and the electron number of the dot takes a fixed value of n , can be obtained as follows.

$$\left(n - \frac{1}{2}\right) \frac{e}{C_g} < V_g < \left(n + \frac{1}{2}\right) \frac{e}{C_g} \quad (10)$$

This condition is also expressed with critical charge Q_c as follows.

$$|Q| < Q_c, \quad (11)$$

where Q_c is expressed as,

$$Q_c = \frac{e}{2} \left(1 + \frac{C_g}{C_t}\right)^{-1}. \quad (12)$$

Free energy change $\Delta F(n, n+1)$ that accompanies a transition of the electron number from n to $n + 1$ is also simply expressed with critical charges Q_c as,

$$\Delta F(n, n+1) = F(n+1) - F(n) = \frac{e}{C_t} (Q_t - Q_c). \quad (13)$$

SET operation (in electronic terms)

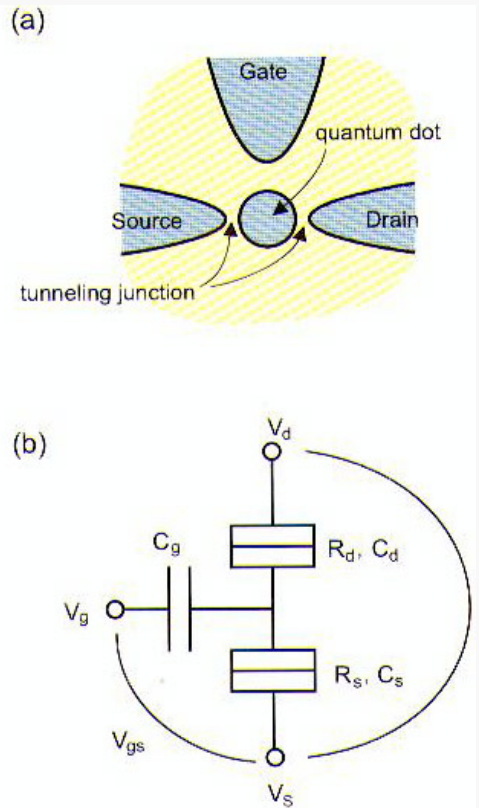


Figure 3:
 (a) Schematic structure of single-electron transistor.
 (b) Equivalent circuit of single-electron transistor.

Operation of Single-Electron Transistors

The operation of single-electron transistors can be described by using Thévenin's theorem and applying derived Eqs. (10) - (12) for a single-electron box.

By using the Thévenin's theorem, the circuit connected to the tunneling junction of the source is transformed to the circuit shown in Figure 4a. From this equivalent circuit and Eq. (10), the condition to maintain the electron number at n in the dot is expressed as

$$\left(n - \frac{1}{2}\right) \frac{e}{C_g + C_d} < \frac{C_g V_g + C_d V_d}{C_g + C_d} < \left(n + \frac{1}{2}\right) \frac{e}{C_g + C_d}, \quad (14)$$

which reduces to

$$\frac{1}{C_d} \left(n e - \frac{e}{2} - C_g V_g \right) < V_d < \frac{1}{C_d} \left(n e + \frac{e}{2} - C_g V_g \right). \quad (15)$$

In the same manner, the circuit connected to the tunneling junction of the drain is transformed to the circuit shown in Figure 4b and the condition to maintain the electron number at n in the dot is expressed as

$$\frac{1}{C_s + C_g} \left(-n e + \frac{e}{2} + C_g V_g \right) > V_d > \frac{1}{C_s + C_g} \left(-n e - \frac{e}{2} + C_g V_g \right) \quad (16)$$

Figure 5a shows the relationship between the drain voltage V_d and the gate voltage V_g , which satisfies the conditions expressed by Eqs. (15) and (16). The gray areas shown in Figure 5a are Coulomb blockade regions, where the Coulomb blockade is effective and the electron number in the dot takes a fixed value indicated in the areas.

On the other hand, in other regions, the quantum dot can take at least two electron numbers. In the green regions shown in Figure 5a the quantum dot can take two electron numbers. For example, in the green region indicated by A, the electron number in the dot is zero or one. More precisely, the electron number of one is preferable for the tunneling junction of the source and the electron number of zero is preferable for the tunneling junction of the drain. Therefore, when a finite positive source-to-drain voltage V_{ds} , indicated by dashed line in Figure 5a, is applied between the source and drain electrodes and the gate voltage is $e/2C_g$, an electron transport process described below is observable. The initial electron number of the dot is assumed to be zero. For the tunneling junction of the source, the electron number of one is preferable so that an electron tunnels from the source to the dot and the electron number in the dot becomes one. However, for the tunneling junction of the drain, the electron number of zero is preferable so that an electron tunnels from the dot to the drain and the electron number in the dot becomes zero. As a result, an electron tunnels from the source to the drain, and source-to-drain current is observable at these bias conditions.

In the same manner, at the gate voltage of $ne/C_g + e/2C_g$, the source-to-drain current I_{ds} is observed, and thus oscillating I_{ds} versus V_g characteristics shown in Figure 5b is observed in single-electron transistors. The oscillating $I_{ds} - V_g$ characteristics are called Coulomb oscillations.

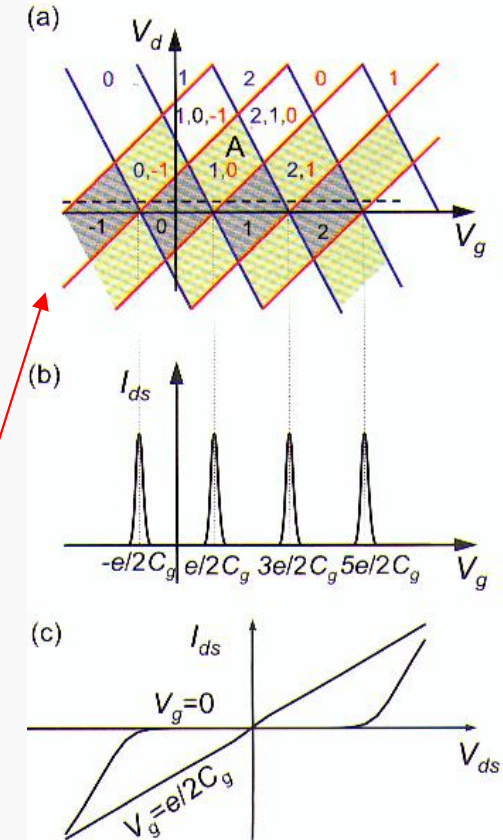
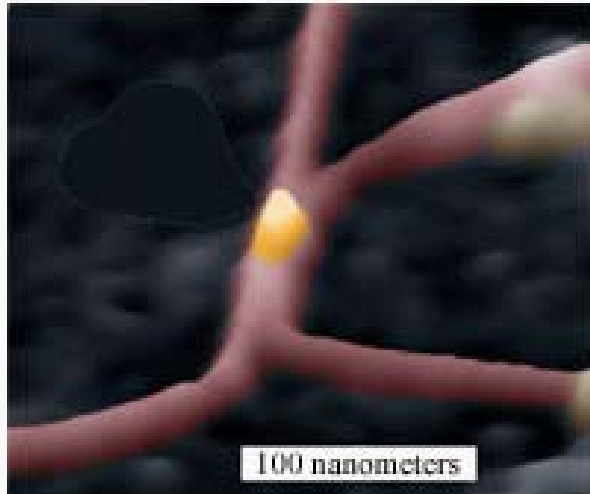


Figure 5:
 (a) Relationship between the drain voltage V_d and the gate voltage V_g , satisfying the conditions expressed by Eqs. (15) and (16). The diamond-shaped structure along the x-axis is called Coulomb diamond.
 (b) source-to-drain current I_{ds} versus gate voltage V_g characteristics of single-electron transistors.
 (c) I_{ds} versus V_{ds} characteristics of single-electron transistors.

A gate is added to change the voltage, i.e., to control the tunneling through the dot

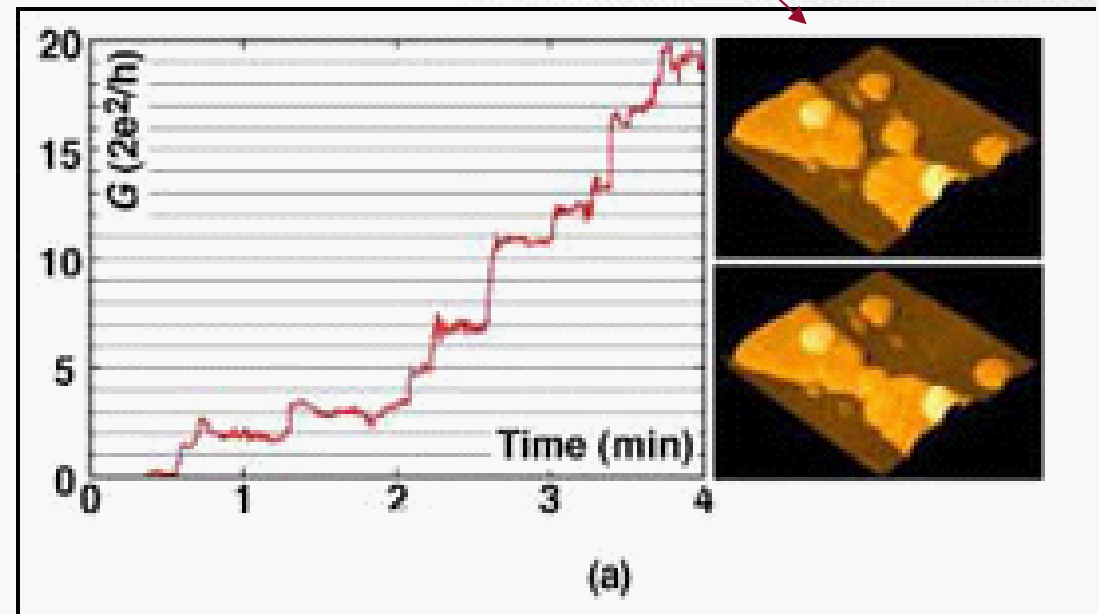
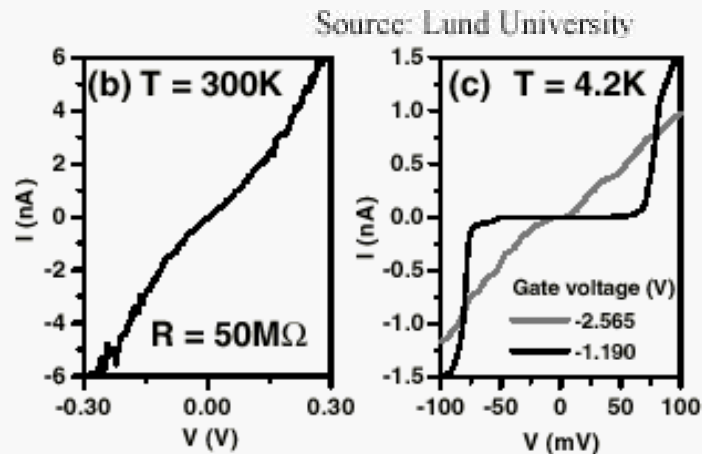
(Unconventional) practical implementations



See Thelander and Samuelson
Nanotechnology 13 108 (2002)

Produced by **scanning probe manipulation** of small metal dots

A tiny speck of gold positioned between two parallel carbon nanotubes forms a transistor that forwards one electron at a time. These single electron transistors could be used to make extremely small, low-power logic circuits.



See Junno et al.,
APL 72 548 (1998); APL 80 (2002)

SET advantages (for the electronics)

Scaling down of electronic device sizes has been the fundamental strategy for improving the performance of ultra-large-scale integrated circuits (ULSIs). Metal-oxide-semiconductor field-effect transistors (MOSFETs) have been the most prevalent electron devices for ULSI applications, and thus the scaling down of the sizes of MOSFETs [1][2] has been the basis of the development of the semiconductor industry for the last 30 years.

However, in the early years of the 21st century, the scaling of CMOSFETs is entering the deep sub-50 nm regime [3]. In this deep-nanoscaled regime, fundamental limits of CMOSFETs and technological challenges with regard to the scaling of CMOSFETs are encountered [4]. On the other hand, quantum-mechanical effects are expected to be effective in these small structured devices. Therefore, in order to extend the prodigious progress of LSI performance, it is essential to introduce a new device having an operation principle that is effective in smaller dimensions and which may utilize the quantum-mechanical effects, and thus provide a new functionality beyond that attainable with CMOSFETs.

Single-electron devices [5][6] are promising as new nanoscaled devices because single-electron devices retain their scalability even on an atomic scale and, moreover, they can control the motion of even a single electron. Therefore, if the single-electron devices are used as ULSI elements, the ULSI will have the attributes of extremely high integration and extremely low power consumption. In this respect, scalability means that the performance of electronic devices increases with a decrease of the device dimensions. Power consumption is roughly proportional to the electron number transferred from voltage source to the ground in logic operations. Therefore, the utilization of single-electron devices in ULSIs is expected to reduce the power consumption of ULSIs.

On the other hand, as for the disadvantages, 1) operations of SET circuits are generally limited to low temperature. This is a negative aspect of the good scalability. In order to operate SET circuits at room temperature, the size of the quantum dot must be much smaller than 10 nm. With the present technology, fabricating a structure smaller than 10 nm is difficult. In addition, 2) SETs have the disadvantage of high output impedance, due to the high resistance of tunnel junctions, which must be much higher than 25.8 k Ω (Eq. (3)). Finally, 3) source-to-drain voltage of SETs should be smaller than gate voltage swing in order to use SETs as gate controlled switching device, because the potential of the dot is easily affected by the source-to-drain voltage. The effect of source-to-drain voltage on the switching characteristics of SETs will be quantitatively evaluated in Sect. 3.2.

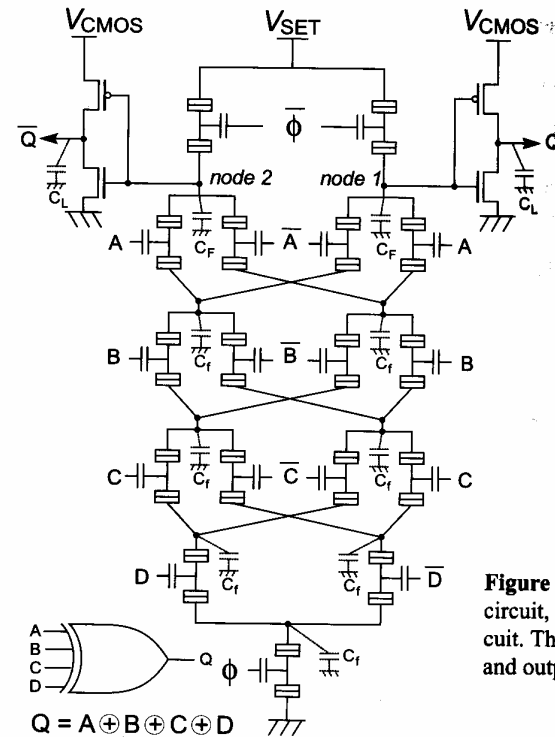


Figure 20: Example of SET logic circuit, four-way exclusive OR circuit. The complementary inputs and outputs are used.

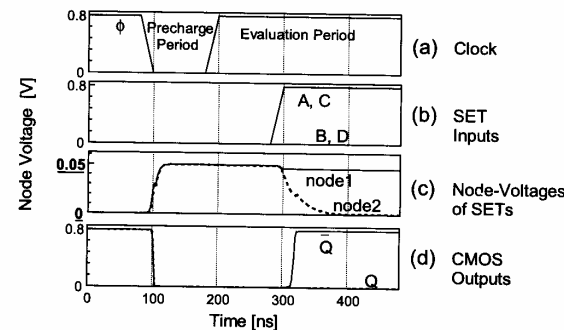
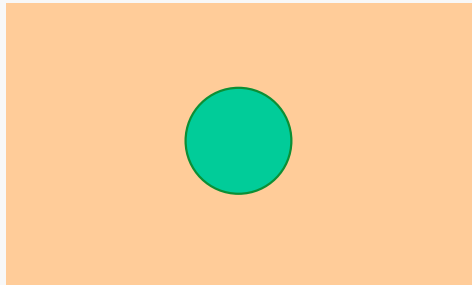


Figure 21: The simulated timing chart of the circuit shown in Figure 20. Here, $C_g = 0.1$ aF, $C_s = C_d = 0.06$ aF, $R_t = 500$ k Ω , $C_i = 10$ fF, $C_F = 1$ fF, $C_f = 50$ aF, $V_{SET} = 50$ mV, and $T = 293$ K.

Example of mixed SET/CMOS technology

Quantum dot / quantum well



A nanosized dot embedded in the “outer” world is a 3D quantum well (spherical quantum box)

Simple 1D case

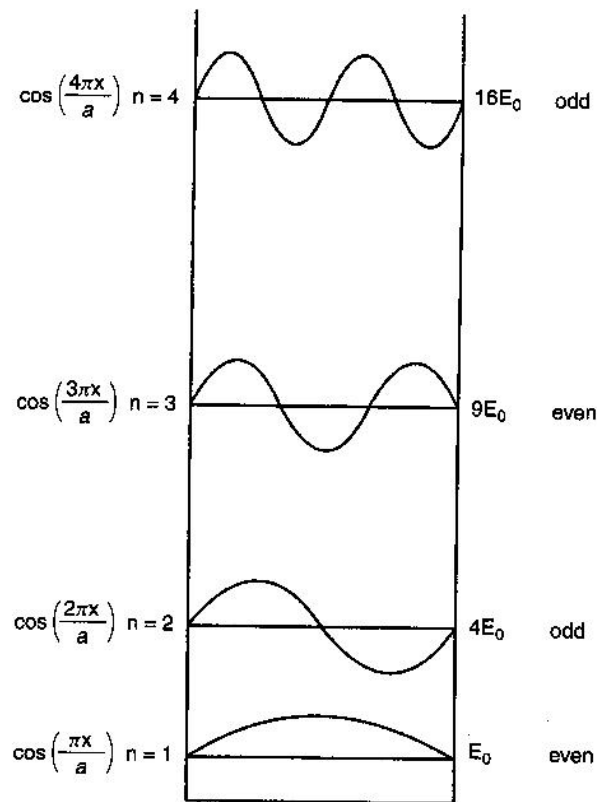


Figure 9.11. Sketch of wavefunctions for the four lowest energy levels ($n = 1-4$) of the one-dimensional infinite square well. For each level the form of the wavefunction is given on the left, and its parity (even or odd) is indicated on the right (From C. P. Poole, Jr., *Handbook of Physics*, Wiley, New York, 1998, p. 289.)

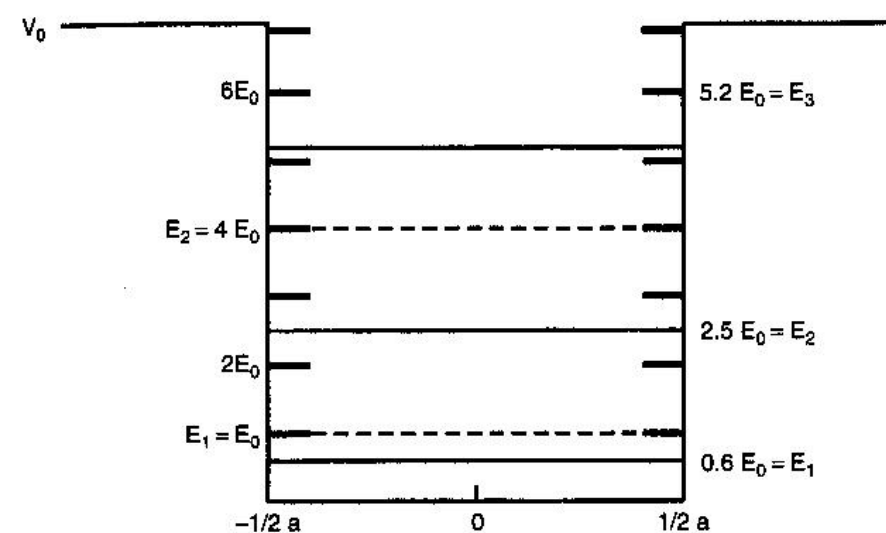


Figure 9.12. Sketch of a one-dimensional square well showing how the energy levels E_n of a finite well (right side, solid horizontal lines) lie below their infinite well counterparts (left side, dashed lines). (From C. P. Poole, Jr., *Handbook of Physics*, Wiley, New York, 1998, p. 285.)

Discrete energy levels appear

Da Poole and Owens
Introduction to Nanotechn.
Wiley (2003)

Size, barrier height, material and energy

A “material discontinuity” is needed to define the well, e.g.: metal/vacuum, metal/oxide, semiconductor/oxide, **semiconductors with different gap energies**

In the actual conditions, the potential barrier is finite, but *few differences with respect to infinite case* (possibility of tunnelling, slight change in level energy, typically a few excited levels can be kept in the well, ...)

Punti quantici (Q.D.). La nanostruttura più difficile da ottenere, ma anche la più complessa per i suoi effetti sulle proprietà ottiche e di trasporto, è quella in cui il confinamento del materiale a “gap” inferiore avviene in tutte e tre le direzioni dello spazio. Dal punto di vista della simmetria di traslazione si può allora dire che la struttura è a dimensionalità zero, e per questo viene chiamata “punto quantico” (Q.D. dall’inglese Quantum Dot). I livelli di energia per gli elettroni e per le buche sono solo livelli discreti, risultanti dal confinamento. Si può ottenere una prima grossolana approssimazione per gli elettroni dal calcolo quantistico degli stati della buca cubica a pareti infinite di lato L ,

$$E_{n_x, n_y, n_z} = E_g + \frac{\pi^2 \hbar^2}{2m^* L^2} (n_x^2 + n_y^2 + n_z^2), \quad (11.92)$$

con $(n_x, n_y, n_z = 1, 2, \dots)$. Si ottiene un simile risultato per le buche, con la separazione tra stati di massa pesante e di massa leggera dovuti al confinamento. Il calcolo preciso, con potenziale finito, richiede anche in questo caso l’uso delle condizioni di continuità al contorno e lo sviluppo della matrice di Luttinger per le buche.

Level energies can be “engineered”

Simple one dimensional case

$$E_n = \hbar^2 k_n^2 / (2 m^*) \quad \text{with } k_n = n 2\pi / L$$

$$E_n = n^2 \hbar^2 \pi / (2 m^* L^2)$$

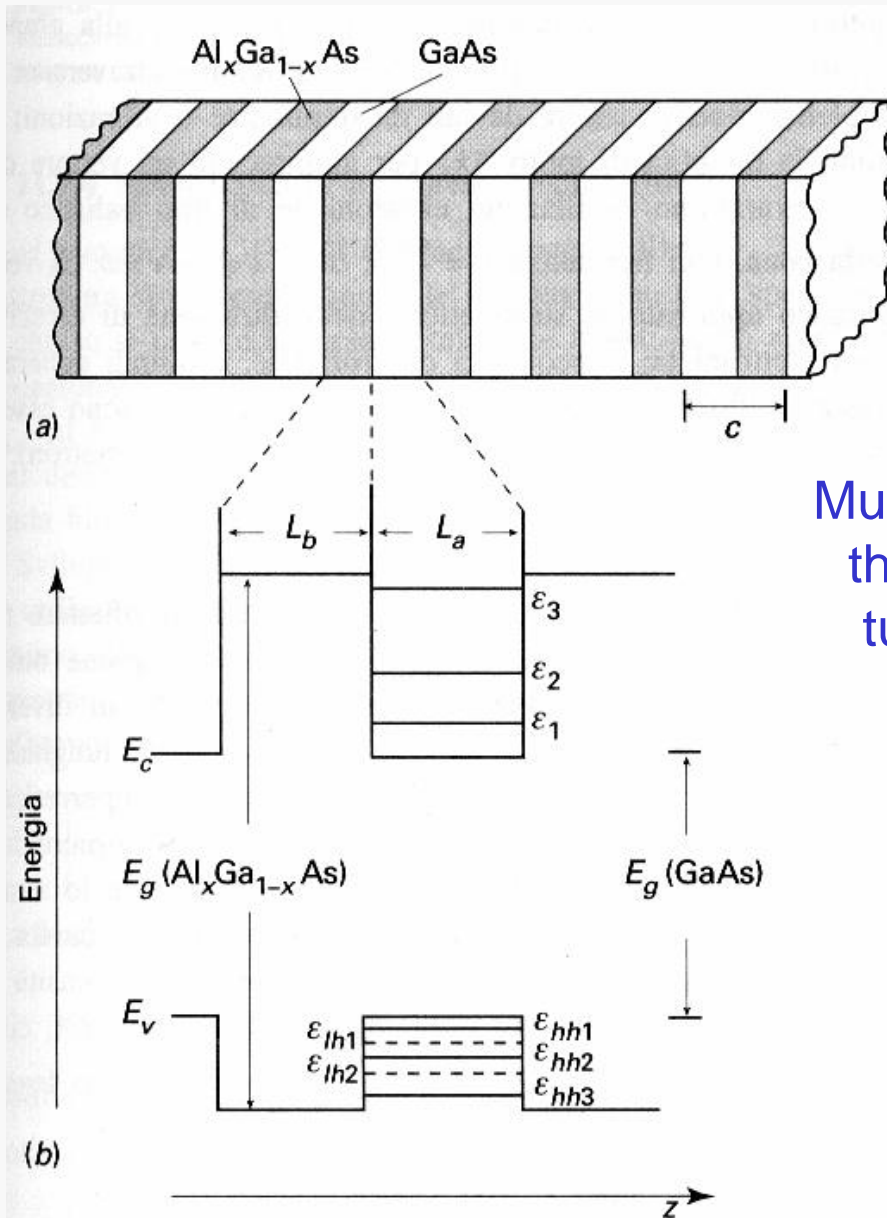
$$\Delta E_n = (2n + 1) \hbar^2 \pi / (2 m^* L^2)$$

material

size

Example: free electron (m_e), width $L=5$ nm: $E_{n=2} - E_{n=1} \sim 1$ eV (even larger for electrons in a semiconductor if $m^* < m_e$)

2D (and 1D) quantum confined structures



Superlattices
(heterostructures): sequence of
layers made of semiconductors
with **different gap energies**

Multiple Quantum Wells: superlattice with layer
thickness large enough to prevent interlayer
tunnelling, i.e., to confine the wavefunction

✓ MQW are “similar” to quantum dots
but quantum confinement occurs only
in one direction (the growth direction of
the thin layers)

✓ Very relevant for **optical properties**
and optoelectronics (we will see!)

Figura 11.31

Schema di un superreticolo formato con $\text{Al}_x\text{Ga}_{1-x}\text{As}/\text{GaAs}$ ($c = na + mb$ è il parametro reticolare nella direzione z).

Da Bassani Grassano,
Fisica dello Stato Solido,
Boringhieri (2000)

Semiconductor quantum dots and SET

Semiconductor Quantum Dot

It should be noted that when the quantum-dot size is comparable with the de Broglie wavelength of the electrons in quantum dots (this situation frequently occurs in the case of semiconductor nanoscaled quantum dots), the energy quantization becomes comparable with the charging energy. In this case, the energy difference due to the addition of a single electron to the dot is given not by the charging energy W_c but by the electron addition energy W_a , which is given by the following formula.

$$W_a = W_c + \Delta W \quad (22)$$

Here ΔW is the quantum energy level difference due to the addition of a single electron to the dot.

As a result, periodicity of Coulomb oscillations is modified as [10],

$$\Delta V_g = \frac{e}{C_g} + \frac{\Delta W}{e} \quad (23)$$

Thus, in quantum dots holding just a few electron, the electron addition energy W_a can no longer be parameterized with W_c , and the Coulomb oscillations are significantly modified by electron-electron interactions and quantum confinement effects. Therefore, in this case, quantum dots are regarded as *artificial atoms* [14].

By utilizing Eq. (23), the energy spectrum of a quantum dot, or an *artificial atom*, can be studied. Tarucha *et al.* have fabricated vertical single-electron transistors (SETs) having circular-disk-shaped dots with double heterostructure barriers and surrounding side gate, shown in Figure 6, and observed, in the transport measurements, atom-like properties such as "magic numbers" and "Hund's first rule" [15], [16], [17].

In the vertical SET, the quantum dot is located in the center of the pillar. The diameter of the dot is a few hundred nanometers and its thickness is about 10 nm. The dot is sandwiched with two non-conducting heterostructure barrier layers, which separate it from conducting material above and below. A negative voltage applied to the side gate around the pillar squeezed the effective diameter of the dot. Consequently, the number of electrons is reduced, one by one, until the dot is completely empty.

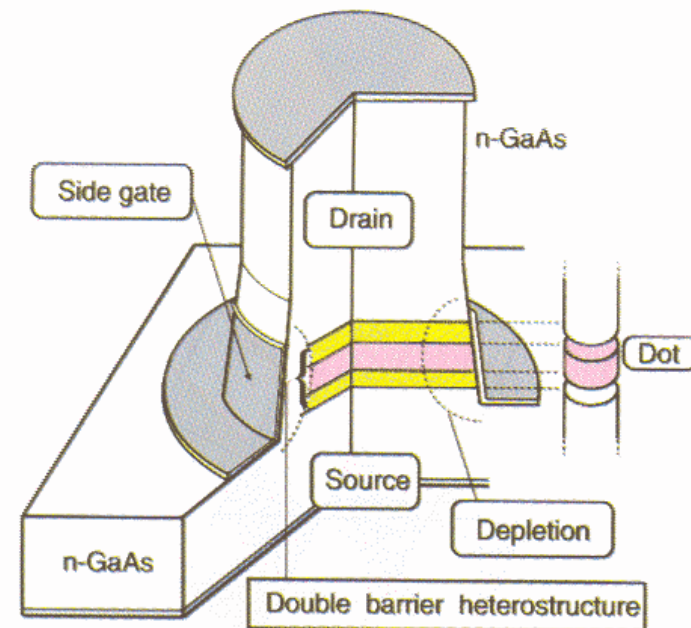
If the lateral confinement has the form of harmonic potential, the eigen-energy $W_{n,l}$ is expressed with radial quantum number n_r ($=0, 1, 2, \dots$) and the angular momentum quantum number l ($=0, \pm 1, \pm 2, \dots$):

$$W_{n,l} = (2n_r + |l| + 1)\hbar\omega_0 \quad (24)$$

where $\hbar\omega_0$ is the lateral confinement energy [16], [17]. Here, the Zeeman effect is neglected. Therefore, it should be noted that each state is spin degenerate.

Vertical SET

Figure 6: Schematic of a quantum dot in a vertical device (After Tarucha *et al.* [17], © 2001 IOP Publishing Co.).



Artificial atom in vertical SET

Figure 7a shows the $I_d - V_g$ characteristics, or Coulomb oscillation characteristics, of the vertical SET. The distance between the consecutive peaks is proportional to W_a , which is the energy difference between the transition point of $(N$ to $N + 1)$ and $(N + 1$ to $N + 2)$ electrons and is equal to the difference of the ionization energy and the electron affinity [18]. The addition energies, W_a 's, extracted from the $I_d - V_g$ characteristics are summarized in the inset of Figure 7a. It should be noted that W_a is not constant, and larger energy is necessary to add an electron to the dot with 2, 6, and 12 electrons. The numbers in this sequence can be regarded as "magic numbers" for a two-dimensional harmonic potential dot [15].

The reason is explained as follows [15], [16], [17]. Figure 7b shows the two-dimensional orbits allowed in the dot. The orbit with the smallest radius corresponds to the lowest energy state ($W_{0,0}$), which has zero angular momentum and can have two electrons with opposite spin. The addition of the second electron thus only costs the charging energy, e^2/C . Extra energy ΔW is necessary to add the third electron, because the electron must go into the next energy state ($W_{0,-1}$, $W_{0,1}$), which has an angular momentum ± 1 and can have four electrons. Therefore, extra energy is again necessary to add the seventh electron. The numbers in the above sequence can be thus regarded as *magic numbers* for a two-dimensional harmonic dot.

In addition, for the filling of electrons in the same orbit, parallel spins are favored by "Hund's first rule". This leads to another series of magic numbers of $N = 4, 9, 16, \dots$ corresponding to the half filling of the second, third, fourth orbits, respectively [17].

Thus, the atomic-like features are successfully observed in the vertical SETs having circular disk quantum dots.

Since the above discussions concerning artificial atoms are based on ref. [16], [17], the interested reader is advised to refer to the original monographs [16], [17] and related articles, such as [15], [19], [20].

Artificial atom-like behavior achieved in specific quantum dot configurations

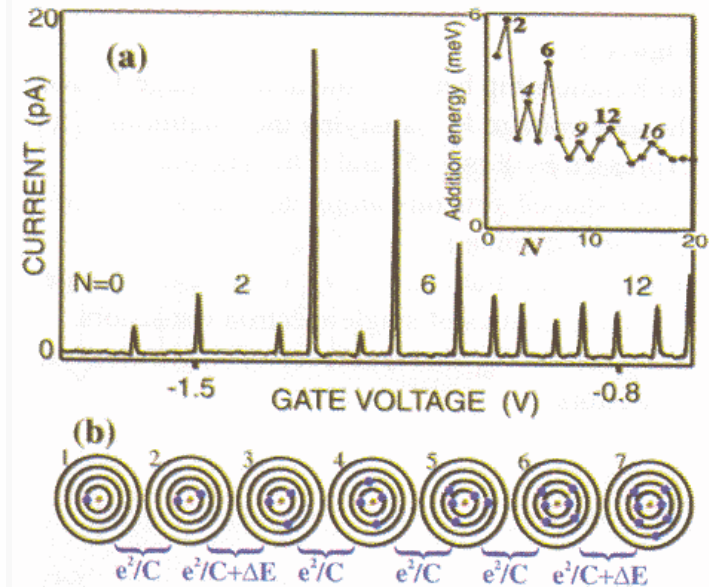
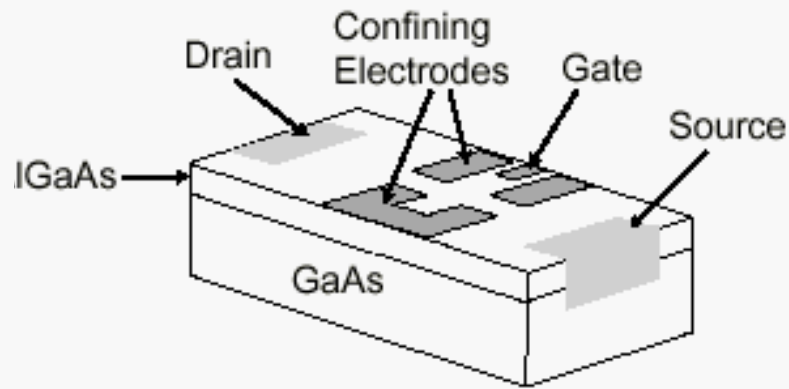
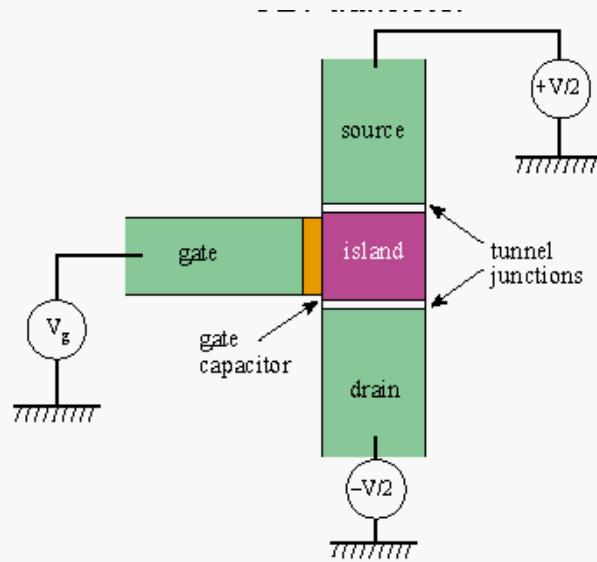


Figure 7: Current flowing through a two dimensional circular quantum dot on varying the gate voltage.

(a) The first peak marks the voltage where the first electron enters the dot, and the number of electrons, N , increases by one at each subsequent peak. The distance between adjacent peaks corresponds to the addition energies (see inset).

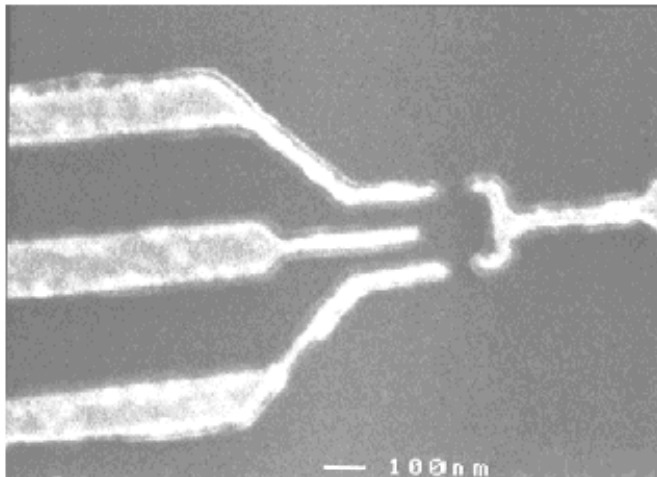
(b) The addition of electrons to circular orbits is shown schematically. The first shell can hold two electrons whereas the second shell can contain up to four electrons. It therefore costs extra energy to add the third and seventh electrons (After Kouwenhoven *et al.* [16], © 2001 IOP Publishing Co.).

SET fabrication (conventional): example I



See Kastner
Ann.Phys 9 885 (2000)

Fig. 1 Schematic drawing of a SET. Wires are connected to source and drain contacts to pass current through the 2DEG at the GaAs/AlGaAs interface. Wires are also connected to the confining electrodes to bias them negatively and to the gate electrode that controls the electrostatic energy of the confined electrons.



SET: three-terminal device similar to MOSFET
but:
single electron capabilities, high speed (ps range), no consumption (*but requires low T!!*)

SET fabrication (conventional): example II

1.4 Fabrication of Single-Electron Devices

There have been a number of reports on the fabrication of single-electron devices. Since single-electron phenomena can be observed in any conductive substances, single-electron devices are fabricated in a variety of materials such as aluminum [24], heterostructures [25], and silicon. However, in order to utilize single-electron devices as elemental devices of LSIs, the realization of single-electron devices made in silicon is essential. This can be achieved if fabrication techniques of nanometer-scaled silicon quantum dots are established.

Regarding silicon quantum dot formation, many approaches have been reported [26], [27], [28], [29], [30], [31] and they are generally categorized into two groups: patterning the silicon quantum dots by fine-lithography techniques and the growth of silicon quantum dots by deposition processes.

Using the former approaches, it is possible to accurately define the structures and positions of quantum dots. For example, Takahashi *et al.* proposed a novel silicon-quantum-dot fabrication process named pattern-dependent oxidation (PADOX) [26]. When a 1-D Si nano-wire, which has wide 2-D Si layers at its ends and is fabricated in silicon-on-insulator (SOI) wafer, is subjected to oxidation process, the oxidation process not only reduces the width and height of the 1-D Si wire, but also constricts the Si wire

at its ends. Since oxygen atoms penetrate not only from the surface oxide layer but also from the backside (the interface of SOI and buried oxide) through the pattern side, oxidation occurs more in the neighborhood of the pattern edges of the 2-D Si layers, as shown in Figure 8. Ono *et al.* have developed the vertical version of PADOX (V-PADOX) [27], shown in Figure 9. In PADOX, laterally broad 2-D regions are essential for tunnel-barrier formation. On the other hand, in V-PADOX, vertically broad, namely thick, 2-D regions are utilized for the tunnel-barrier formation. The advantage of the V-PADOX is that the V-PADOX makes it possible to form two tiny islands in a small area by utilizing not a lithographic process but the oxidation process, which induces the accumulation of stress in small structures. Thus, by utilizing V-PADOX, two SETs can be fabricated in an extremely small area, as shown in Figure 10.

The latter approaches are favorable from the viewpoints of throughput and fabricated quantum-dot sizes. In fact, Yano *et al.* successfully fabricated the room-temperature operating silicon single-electron memory by using the formation process of thin poly-silicon film, in which an array of 10-nm grains is naturally formed [28]. Tiwari *et al.* reported single-electron memory having Si nanocrystal storage [29].

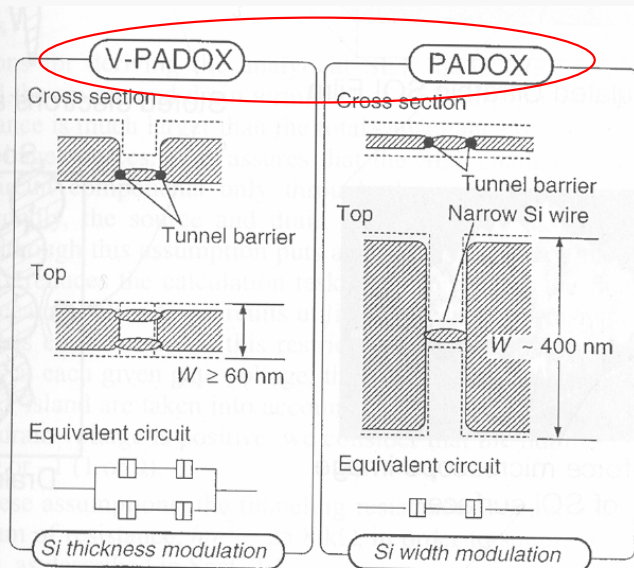


Figure 9: Si patterns and the corresponding circuits for V-PADOX and PADOX. In the cross-sectional and top views, broken lines represent preoxidation Si patterns and hatched regions represent islands and leads after oxidation (After Ono *et al.* [27], © 2000 IEEE).

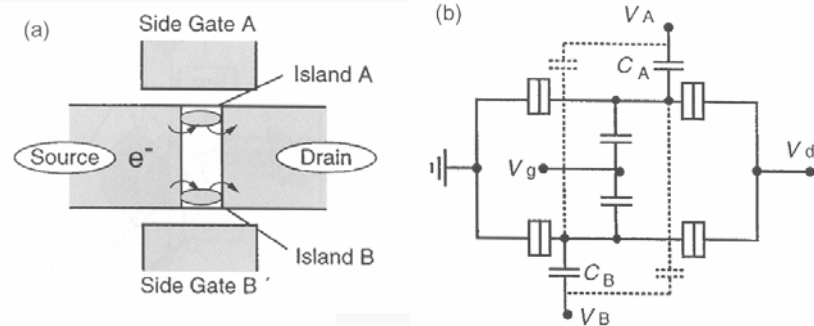


Figure 10: Fabrication of two SETs. (a) Top view of the structure. (b) Equivalent circuit (After Ono *et al.* [27], © 2000 IEEE).

(Anisotropic) oxidation used to obtain Si quantum dots

SET fabrication (conventional): example III

Uchida *et al.* proposed another approach, where slight etching of an ultrathin SOI film with an alkaline-based solution is utilized [30], [32]. The proposed device structure is schematically illustrated in Figure 11a. As shown in the figure, the device structure is almost the same as that of conventional SOI-MOSFETs, but the SOI film has two key features: 1) its surface is intentionally undulated in nanoscaled dimensions as shown in Figure 11b by utilizing an alkaline-based solution; 2) the channel SOI thick-ness is thinned to a few nanometers. The nanoscaled undulation in the ultrathin film results in the formation of nanoscaled potential fluctuations due to the difference of quantum confinement effects from one part to another. Consequently, both the narrow electron channel through potential valleys and small potential pockets, storing memory information, are formed in the film as shown in Figure 11c. Since potential fluctuation still exists in the narrow channel, the channel effectively splits into several quantum dots. The quantum dots included in the channel are the origin of the SET operation. Thus, the device works as a single-electron transistor with nonvolatile memory function. Since the fabrication process of this SET is compatible with that of CMOSFETs, SET/CMOS hybrid circuit is fabricated on a chip, as shown in Figure 12, and its operation is successfully demonstrated even at room temperature [32].

**Nanosized “undulation”
(obtained by mild etching)
lead to a sequence of
quantum dots**

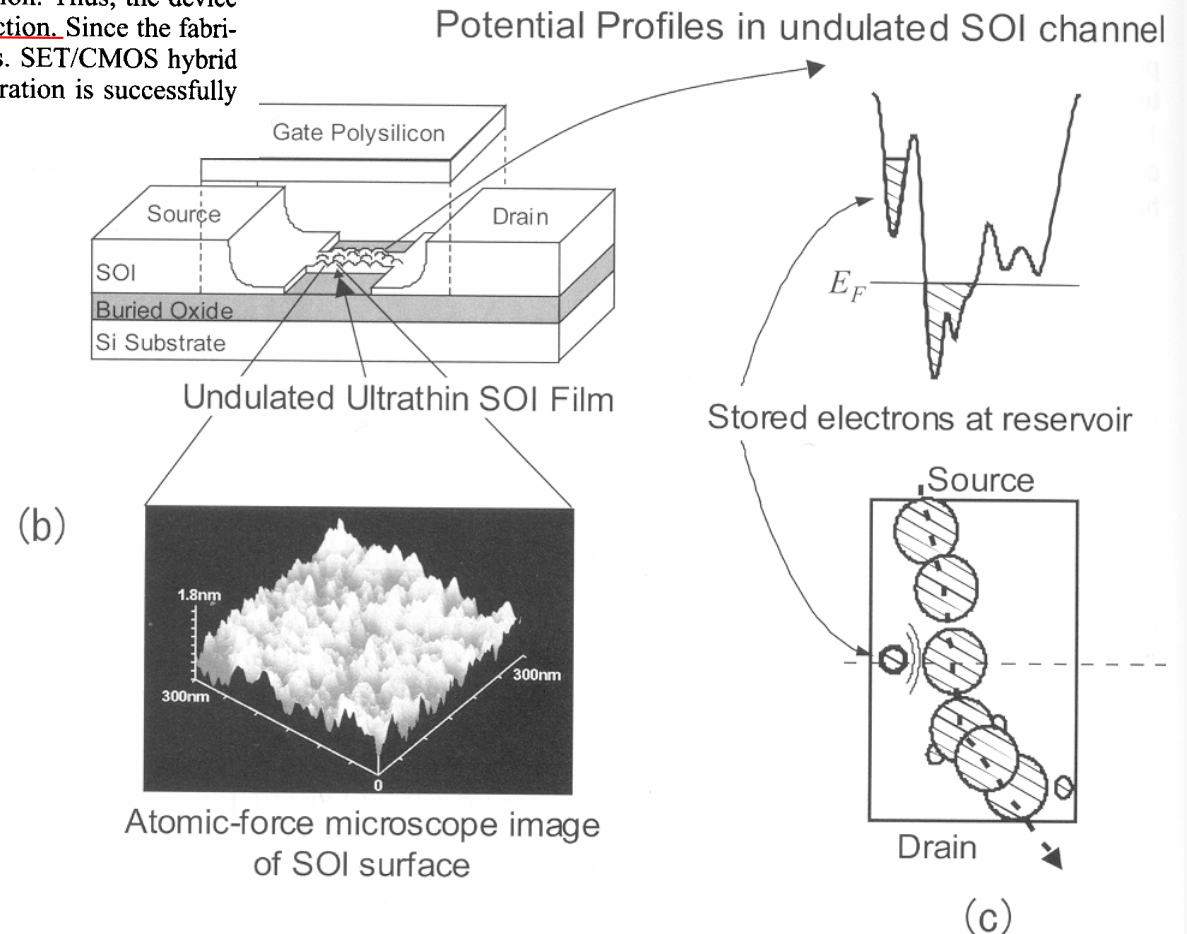


Figure 11: Device structure and operation principle of single-electron transistor with nonvolatile memory function.

Reminder of tunnel effect I

For the barrier potential of (6-45), we know from the qualitative arguments of the last chapter that acceptable solutions to the time-independent Schroedinger equation should exist for all values of the total energy $E \geq 0$. We also know that the equation breaks up into three separate equations for the three regions: $x < 0$ (left of the barrier), $0 < x < a$ (within the barrier), and $x > a$ (right of the barrier). In the regions to the left and to the right of the barrier the equations are those for a free particle of total energy E . Their general solutions are

$$\begin{aligned} \psi(x) &= Ae^{ik_1x} + Be^{-ik_1x} & x < 0 \\ \psi(x) &= Ce^{ik_{II}x} + De^{-ik_{II}x} & x > a \end{aligned} \quad (6-46)$$

where

$$k_1 = \frac{\sqrt{2mE}}{\hbar}$$

In the region within the barrier, the form of the equation, and of its general solution, depends on whether $E < V_0$ or $E > V_0$. Both of these cases have been treated in the previous sections. In the first case, $E < V_0$, the general solution is

$$\psi(x) = Fe^{-k_{II}x} + Ge^{k_{II}x} \quad 0 < x < a \quad (6-47)$$

where

$$k_{II} = \frac{\sqrt{2m(V_0 - E)}}{\hbar} \quad E < V_0$$

In the second case, $E > V_0$, it is

$$\psi(x) = Fe^{ik_{III}x} + Ge^{-ik_{III}x} \quad 0 < x < a \quad (6-48)$$

where

$$k_{III} = \frac{\sqrt{2m(E - V_0)}}{\hbar} \quad E > V_0$$

Note that (6-47) involves real exponentials, whereas (6-46) and (6-48) involve complex exponentials.

Since we are considering the case of a particle incident on the barrier from the left, in the region to the right of the barrier there can be only a transmitted wave as there is nothing in that region to produce a reflection. Thus we can set

$$D = 0$$

In the present situation, however, we cannot set $G = 0$ in (6-47) since the value of x is limited in the barrier region, $0 < x < a$, so $\psi(x)$ for $E < V_0$ cannot become infinitely large even if the increasing exponential is present. Nor can we set $G = 0$ in (6-48) since $\psi(x)$ for $E > V_0$ will have a reflected component in the barrier region that arises from the potential discontinuity at $x = a$.

We consider first the case in which the energy of the particle is less than the height of the barrier, i.e., the case:

$$E < V_0$$

In matching $\psi(x)$ and $d\psi(x)/dx$ at the points $x = 0$ and $x = a$, four equations in the arbitrary constants A, B, C, F , and G will be obtained. These equations can be used to evaluate B, C, F , and G in terms of A . The value of A determines the amplitude of the eigenfunction, and it can be left arbitrary. The form of the probability density corresponding to the eigenfunction obtained is indicated in Figure 6-14 for a typical situation. In the region $x > a$ the wave function is a pure traveling wave and so the probability density is constant, as for $x > 0$ in Figure 6-10. In the region $x < 0$ the wave function is principally a standing wave but has a small traveling wave component because the reflected traveling wave has an amplitude less than that of the

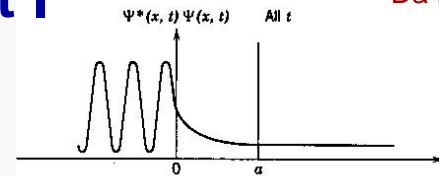


Figure 6-14 The probability density function $\Psi^*\Psi$ for a typical barrier penetration situation.

incident wave. So the probability density in that region oscillates but has minimum values somewhat greater than zero, as for $x < 0$ in Figure 6-10. In the region $0 < x < a$ the wave function has components of both types, but it is principally a standing wave of exponentially decreasing amplitude, and this behavior can be seen in the behavior of the probability density in the region.

The most interesting result of the calculation is the ratio T , of the probability flux transmitted through the barrier into the region $x > a$, to the probability flux incident upon the barrier. This transmission coefficient is found to be

$$T = \frac{v_1 C^* C}{v_1 A^* A} = \left[1 + \frac{(e^{k_{II}a} - e^{-k_{II}a})^2}{16 \frac{E}{V_0} \left(1 - \frac{E}{V_0}\right)} \right]^{-1} = \left[1 + \frac{\sinh^2 k_{II}a}{4 \frac{E}{V_0} \left(1 - \frac{E}{V_0}\right)} \right]^{-1} \quad (6-49)$$

where

$$k_{II}a = \sqrt{\frac{2mV_0a^2}{\hbar^2} \left(1 - \frac{E}{V_0}\right)} \quad E < V_0$$

If the exponents are very large, this formula reduces to

$$T \approx 16 \frac{E}{V_0} \left(1 - \frac{E}{V_0}\right) e^{-2k_{II}a} \quad k_{II}a \gg 1 \quad (6-50)$$

as can be verified with ease. When (6-50) is a good approximation, T is extremely small.

These equations make a prediction which is, from the point of view of classical mechanics, very remarkable. They say that a particle of mass m and total energy E , incident on a potential barrier of height $V_0 > E$ and finite thickness a , actually has a certain probability T of penetrating the barrier and appearing on the other side. This phenomenon is called *barrier penetration*, and the particle is said to *tunnel* through the barrier. Of course, T is vanishingly small in the classical limit because in that limit the quantity $2mV_0a^2/\hbar^2$, which is a measure of the opacity of the barrier, is extremely large.

We shall discuss barrier penetration in detail shortly, but let us first finish describing the calculations by considering the case in which the energy of the particle is greater than the height of the barrier, i.e., the case:

$$E > V_0$$

In this case the eigenfunction is oscillatory in all three regions, but of longer wavelength in the barrier region, $0 < x < a$. Evaluation of the constants B, C, F , and G by application of the continuity conditions at $x = 0$ and $x = a$, leads to the following formula for the transmission coefficient

$$T = \frac{v_1 C^* C}{v_1 A^* A} = \left[1 - \frac{(e^{ik_{III}a} - e^{-ik_{III}a})^2}{16 \frac{E}{V_0} \left(\frac{E}{V_0} - 1\right)} \right]^{-1} = \left[1 + \frac{\sin^2 k_{III}a}{4 \frac{E}{V_0} \left(\frac{E}{V_0} - 1\right)} \right]^{-1} \quad (6-51)$$

$$k_{III}a = \sqrt{\frac{2m}{\hbar^2} \frac{V_0}{V_0} \left(\frac{E}{V_0} - 1\right)} \quad E > V_0$$

MP16

Depends on E/V_0 and a

Reminder of tunnel effect II

Da Eisberg Resnick, Quantum Physics
Wiley (1985)

Table 6-2. A Summary of the Systems Studied in Chapter 6

Name of System	Physical Example	Potential and Total Energies	Probability Density	Significant Feature
Zero potential	Proton in beam from cyclotron			Results used for other systems
Step potential (energy below top)	Conduction electron near surface of metal			Penetration of excluded region
Step potential (energy above top)	Neutron trying to escape nucleus			Partial reflection at potential discontinuity
Barrier potential (energy below top)	α particle trying to escape Coloumb barrier			Tunneling
Barrier potential (energy above top)	Electron scattering from negatively ionized atom			No reflection at certain energies
Finite square well potential	Neutron bound in nucleus			Energy quantization
Infinite square well potential	Molecule strictly confined to box			Approximation to finite square well
Simple harmonic oscillator potential	Atom of vibrating diatomic molecule			Zero-point energy



Single well tunneling

Tunneling relevant in inter dot transport

More on tunneling through quantum dots

Da R. Waser Ed., Nanoelectronics and information technology (Wiley-VCH, 2003)

2.1.1 Tunneling Through a Single Barrier

We consider the tunneling probability through a single potential barrier Figure 2. The experimental equivalent is an AIAs barrier embedded in GaAs. The electron transmission probability as a function of the electron energy was calculated according to Eq. (15) for three different thicknesses of the barriers. First we observe a finite transmission probability for electrons far below the potential height of 1.0 eV. This effect is known as the tunneling effect. The electron wave function in front of the barrier leaks out through the barrier and leads to a finite transmission. The smaller the barrier thickness, the higher is the tunneling probability of the electrons with energies below the potential energy of the barrier. In a classical picture the electrons could not penetrate the barrier. In addition we see a modulation of the transmission probability for electrons at energies above the 1.0 eV barrier height. In this region interference effects of transmitted and reflected electron waves appears, which demonstrate the wave character of the electrons.

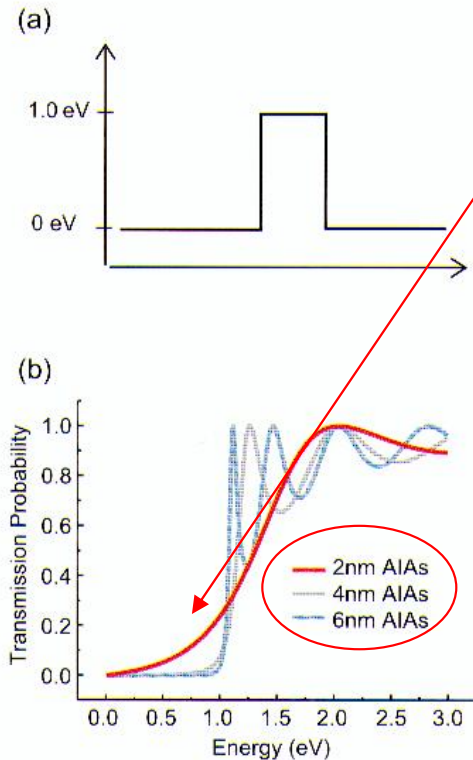


Figure 2: Schematic band diagram of a single AlAs barrier (a) and the corresponding tunneling transmission probability for different barrier thicknesses (b).

2.1.2 Tunneling Through a Double Barrier Structure

To see the difference between the tunneling effect through a single barrier and the resonant tunneling effect, we discuss the case of a double barrier structure (see Figure 3). We consider two 4 nm thick AlAs barriers separated by a 5 nm GaAs well. In contrast to the transmission through a single barrier now electrons with very low energies can cross the double barrier structure with a transmission probability of 1. Three additional very sharp maxima appear below 1 eV in Figure 3b: they could be interpreted as quasi-bound states with a very narrow energetic bandwidth, through which electrons can tunnel like

through open channels in the barrier. This is at first astonishing and not compatible with a sequential tunneling picture. In a sequential transport picture we would expect that the transmission probability through two barriers is very much smaller than through one barrier because the transmission through the first barrier is already much below 1. A completely new quantum mechanical system has been developed which can not be described by the behaviour of each single system. This may also be a drawback for quantum devices in general. Quantum mechanical devices can therefore not be placed extremely close to each other without changing the characteristics of the single device.

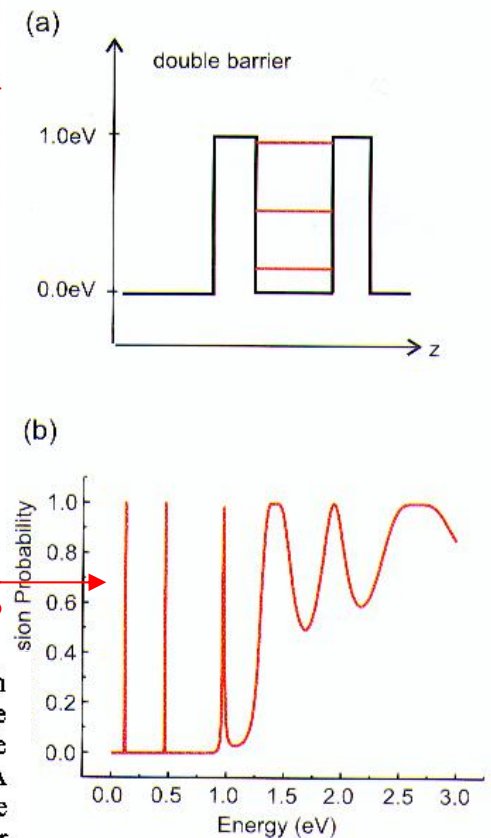


Figure 3: Schematic band diagram of a double barrier structure of AlAs embedded in GaAs (a) and the corresponding tunneling transmission probability (b).

Single barrier

“Resonances” may appear corresponding to the positions of the quantum dot energy levels

Double barrier

Resonant Tunneling Diode (RTD) I

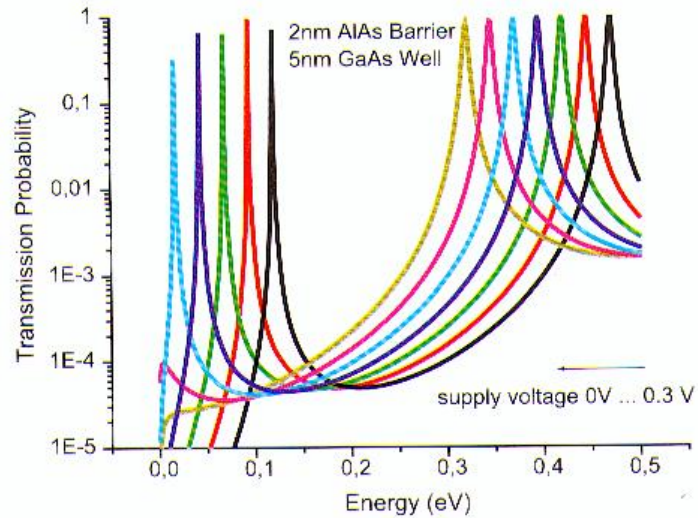
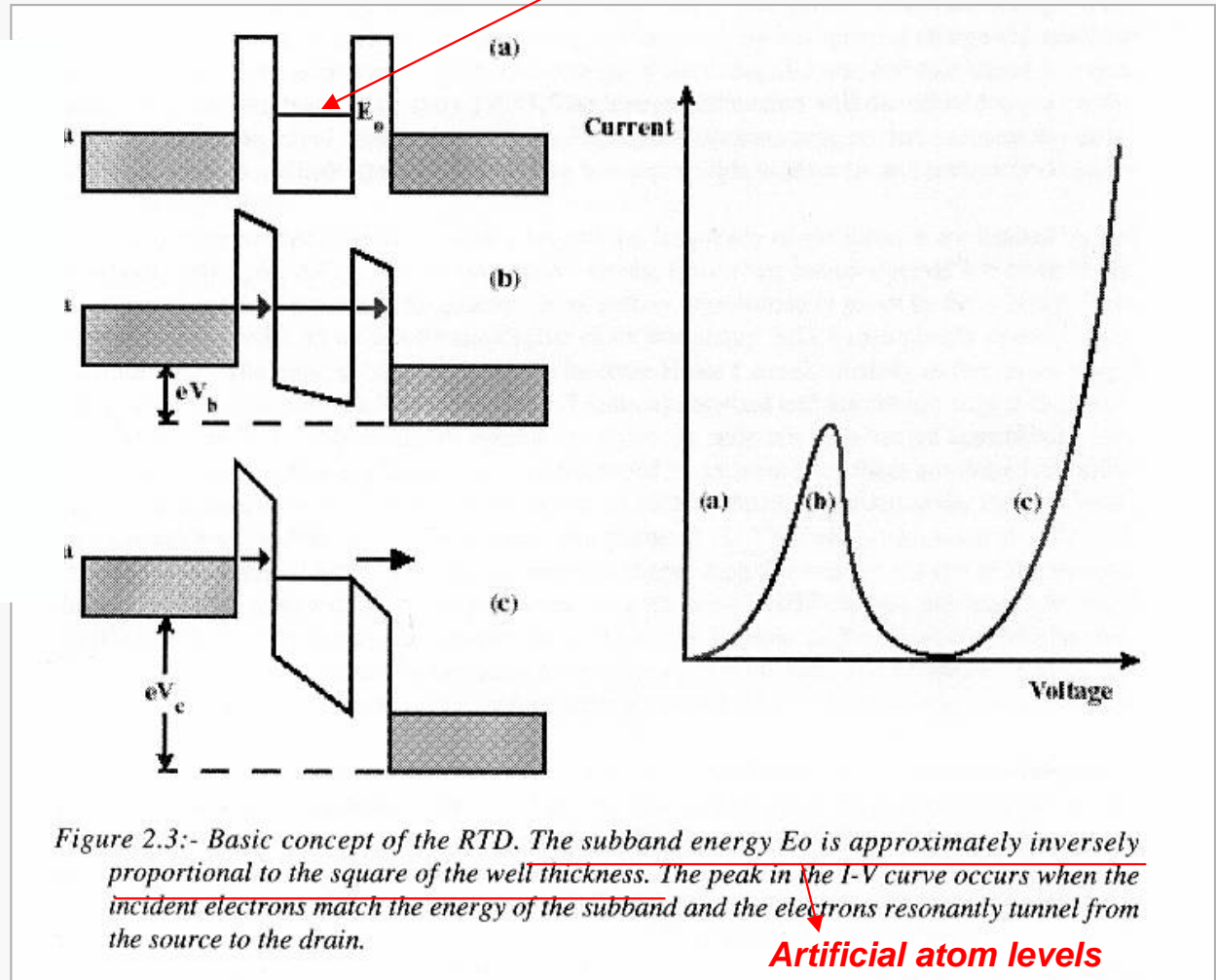


Figure 5: Transmission probability of a double barrier structure at different supply voltages.



RTD proposed as a system with extremely high speed and low consumption

Resonant Tunneling Diode (RTD) II

3.2 Current-Voltage Characteristics

The current density at a certain supply voltage can be calculated using the transmission probability together with the corresponding actual electron occupation densities. For the example of a double barrier structure the highly doped supply layers left and right of the double barrier can be described as free electron gases. The current density is obtained as the difference between the current density flux from the left to the right side of the double barrier and that one in the opposite direction. After Tsu *et al.* [2] this can be written as:

$$j = \frac{2|e|}{(2\pi)^3} \int_0^\infty dk_z \int_0^\infty dk_{\parallel} (f_l(W) - f_r(W + eV)) T_c(W_z, V) \frac{1}{\hbar} \frac{\partial W_z}{\partial k_z} \quad (18)$$

where the coherent transmission probability $T_c(W_z, V)$ is a function of the supply voltage V and energy in z direction W_z , f_l and f_r are the Fermi distributions, left and right of the double barrier, and k_{\parallel} and k_z denote the parallel- and z -component of the momentum, respectively. The integration of Eq. (18) leads to the current density expression containing the supply function:

$$j(V) = \frac{4\pi|e|m^*k_B T}{\hbar^3} \int_0^\infty dW_z T_c(W_z, V) \ln \left| \frac{1 + \exp\left(\frac{W_F - W_z}{k_B T}\right)}{1 + \exp\left(\frac{W_F - W_z - eV}{k_B T}\right)} \right| \quad (19)$$

For an accurate calculation of the transmission probability the real potential profile across the device is required. The potential Φ includes the device energy band offset of the heterojunctions, the voltage drop across the structure and the contributions from the doping and mobile charges. By coupling the effective mass Schrödinger equation with the Poisson equation the potential Φ is obtained in a self-consistent manner.

Calculations of current voltage characteristics lead to a deeper insight into the physics of resonant tunneling diodes and are necessary in the device designing. A typical calculation is shown in Figure 6. The main characteristic feature is the existence of a negative differential resistance region which is the base of most of the RTD-applications. From the application point of view important parameters are: the peak current density, the valley current density, the peak to the valley current density ratio (PVR) and the peak voltage.

The peak current density decreases exponentially with the barrier thickness as the halfwidth of the resonance Eq. (16).

While the absolute peak-current densities resulting from simulations are in good agreement with experimental data, the calculated valley current densities are one or more orders of magnitude lower than the experimental ones. For AlAs/GaAs or AlAs/InGaAs diode structures on GaAs the experimental PVRs at room temperature are in the order of 6. The predicted PVR values from simulations are more than one order of magnitude higher (see Figure 7b and [10]). The reason for this discrepancy is the neglect of scattering effects in the calculation. Scattering effects broaden the resonance in the transmission probability while simultaneously damping it. The peak current density is nearly not sensitive to scattering effects but the valley current and the PVR are very strongly influenced.

An appropriate scattering model is based on the Breit-Wigner generalization of the Lorentzian form of the resonant transmission probability. Within this formalism resonant tunneling in one dimension is studied by Stone *et al.* [3] who derived the total transmission probability in the presence of inelastic scattering for a symmetric structure as:

$$T_{\text{tot}} = \frac{\frac{1}{4} \Gamma_0 \Gamma}{(W - W_r)^2 + \frac{1}{4} \Gamma^2}$$

where Γ_0 is the half width of the resonance in the coherent transmission probability $\Gamma = \Gamma_0 + \Gamma_i$ is the total resonance half width, Γ_i representing the contribution arising due to the inelastic scattering. Büttiker [4] has interpreted this total probability as a sum of a coherent and sequential transmission probabilities

$$T_{\text{tot}} = T_c + T_i$$

In this picture of scattering the fraction of carriers penetrating the structure $T_c / T_{\text{tot}} = \Gamma_0 / \Gamma$ and the fraction of carriers traversing the structure sequentially $T_i / T_{\text{tot}} = \Gamma_i / \Gamma$. From these results one can infer that the smaller the elastic scattering probability Γ_i is the amount of scattering needed to make the sequential tunneling dominant. This means that in tunneling diodes with thick barriers (sharp resonance) despite of a small scattering probability, considerable sequential tunneling will be observed. Furthermore, Eq. (20) can be interpreted as a folding of the transmission probability (Eq. (20)) with $\Gamma_i = 0$ with a normalized Lorentzian width Γ_i . In current density calculations this mechanism conserves the peak current density but affects the valley current very strongly resulting in lower PVR values. In this kind of treatment of $I - V$ curves the effect of scattering is used as a fitting parameter to determine the resonance broadening at room temperature. For a typical RTD with AlAs barriers and a 5 nm GaAs quantum well a resonance halfwidth of about 10 meV at room temperature was found (see [5]).

From the theoretical point of view this treatment of scattering is not sufficient. Therefore a more complex approach is needed. In an enhanced calculation the non-equilibrium Green-function theory is the base of the calculations in which sequential tunneling, incoherent and inelastic scattering, and the band structure is considered. Stone *et al.* [6] have developed a complex simulation package in which most of the effects are taken into account. A real-space tight binding formulation provides a fast and accurate synthesis of heterostructures on an atomic scale. It implies the consideration of inter-valley and inter-band transitions and gives a sophisticated description in the gap-region ("band-wrapping"). This approach was the base for the device simulation package NEMO (NanoElectronic Modeling) that simulates a wide variety of quantum devices, including RTDs, HEMTs, HBTs, superlattice diodes.

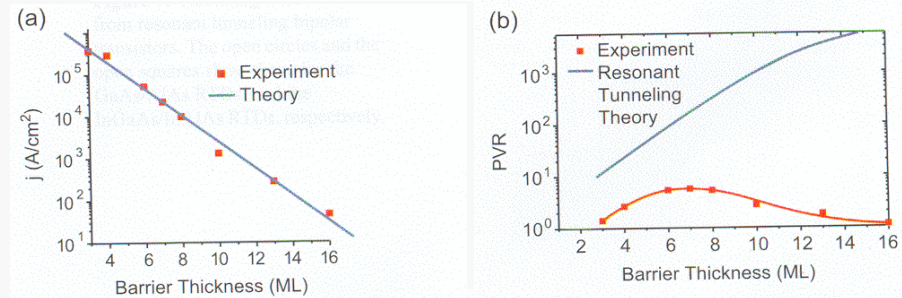
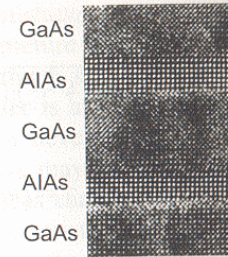
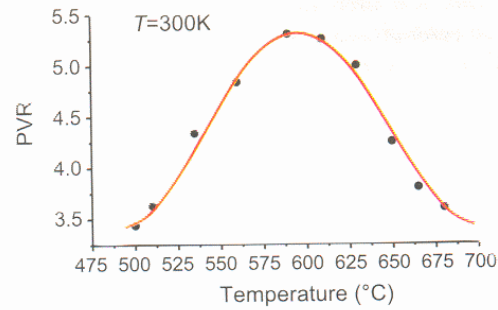


Figure 7: Comparison between theory according to Eq.(19) and experiment for a GaAs resonant tunneling diode (a) peak current density, (b) PVR.

Resonant Tunneling Diode (RTD) III

Figure 8: PVR of an AlAs/GaAs double barrier structure as a function of growth temperature (left). The optimum growth temperature of about 600 °C corresponds to the best quality of the interface in the HRTEM picture (right).



Dependence on fabrication parameters (interface issues)

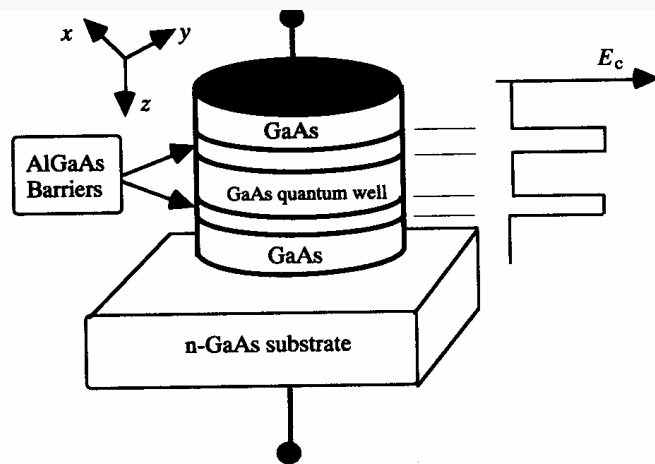
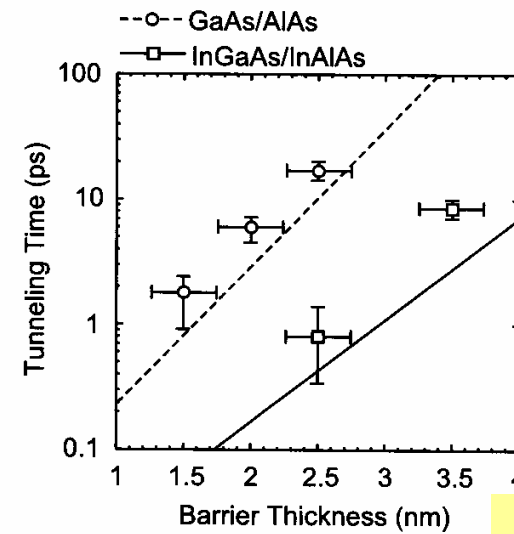


fig. 6.1.1. Resonant tunneling device. A GaAs layer a few nanometers thick is sandwiched between two AlGaAs barrier layers of similar thickness. Adapted with permission from Fig. 2 of F. Capasso and S. Datta (1990), *Physics Today*, **43**, 74.

Example of RTD structure



Huge speed!

Figure 9: Tunneling time obtained from resonant tunneling bipolar transistors. The open circles and the open squares show those for the GaAs/AlAs RTDs, and the InGaAs/InAlAs RTDs, respectively.

Conclusions

- ✓ The ability to control single electrons has a huge appeal, because of potential advantages in terms of operation speed, power consumption, miniaturization and efficiency
- ✓ Single electrons are “felt” by nanosized structures: a metal nanosized capacitor can be tunneled only when a proper potential is established (Coulomb staircase)
- ✓ Coulomb staircase is a manifestation of a quantum effect related to the small dimensions of the structure and to the discrete nature of the electric charge
- ✓ Coulomb blockade can be exploited also to produce three terminal devices (SET)
- ✓ Double barrier tunneling through a quantum dot is also a single electron process exploitable to produce a class of novel diodes (RTDs)